# Suppression of backscattering induced noise by the sideband locking technique in a resonant fiber optic gyroscope

**Ning Liu (刘 宁), Yanxiong Niu (牛燕雄), Lishuang Feng (冯丽爽)*, Hongchen Jiao (焦洪臣), and Xiao Wang (王 潇)**

*School of Instrumentation Science and Opto-electronics Engineering, Beihang University, Beijing 100191, China*

**Corresponding author: fenglishuang_cn@hotmail.com*

Received October 13, 2017; accepted November 23, 2017; posted online December 19, 2017

Polarization fluctuation induced noise and backscattering-induced noise are the dominant noises in resonant fiber optic gyroscopes. This Letter proposes a new method to suppress the carrier and backscattering induced noise by the sideband locking technique. Besides choosing an optimized modulation depth and different clockwise and counterclockwise modulation frequencies, the sideband is locked to the cavity resonance. With the proper modulation frequency, the carrier frequency component locates at a position far away from the resonant frequency, and then it is suppressed by the cavity itself, which can be taken as a bandpass filter. The amplitude of the carrier frequency can be suppressed by 20–25 dB additionally by the cavity and the total intensity suppression ratio can reach 115.74 dB. The backscattering induced noise can be eliminated for the adoption of different frequencies. The method can realize a stable and high suppression ratio without high requirements for parameter accuracy or device performance.

*OCIS codes: 060.2800, 010.1350, 060.2370, 120.4640, 120.5790.*

*doi: 10.3788/COL201816.010608.*

The resonant fiber optic gyroscope (RFOG) is a promising angular velocity sensor based on the Sagnac effect[1,2] that has great advantages in miniaturization and integration over many gyroscopes[3,4]. The RFOG suffers mainly from polarization fluctuation induced noise and backscattering induced noise[5], and many countermeasures have been developed against the latter noise. Sanders *et al.* reduced the backscattering induced noise greatly by phase modulating one of the input beams of the passive ring resonator[6]. Similarly, Meyer *et al.* adopted the method in a passive fiber-optic ring resonator by applying a sinusoidal voltage to piezoelectric ceramic (PZT), around which one input fiber was wrapped to realize phase modulating[7]. In these cases, to suppress the carrier, extremely high accuracy in the adjustment of the modulation index is required. The interference intensity between the signal and the backscattering varies with the thermal fluctuation of the cavity length, and the cavity length modulation technique was proposed[8]. Binary phase shift keying (BPSK)[9,10] was proposed to eliminate the backscattering noise by modulating the input beam, but the acousto-optic modulator used in the system does not meet the RFOG requirements for miniaturization and integration. Based on BPSK, ternary phase shift keying (TPSK) was proposed[11,12] to improve the performance of BPSK, which is degraded by the residual transient of the thermo-optic (TO) modulator. To further suppress the carrier, the double phase modulation technique is adopted, where both a clockwise (CW) and counterclockwise (CCW) sinusoidal voltage with an accurate amplitude is applied on the phase modulators[13,14]. Hybrid waves composed of triangle waves and sawtooth waves were also used to suppress backreflection noise due to facet reflection[15]. Another method, which is called integer period sampling (IPS), is introduced by Wang to minimize the sampling error caused by backreflection[16]. It has difficulties in sampling an exact integer period while the phase of the signal changes irregularly. Some countermeasures, such as modulating the phase of the input beam, require an extremely high modulating accuracy, while some methods introduce unsuitable devices or are hard to implement. In this Letter, based on some of above methods, we first propose sideband locking with different modulation frequencies to realize multi-suppression of carrier and backscattering induced noise. Except for the modulation of phase with proper parameters, the most significant characteristic is that the carrier and backscattering induced noise are both suppressed by the self-characteristic of the cavity. It has no requirements for high accuracy of parameters, and is not limited to the performance of the device. Through the suppression by the cavity itself, the method can realize a stable and high suppression ratio (SPR).

The scheme to realize a high SPR of carrier and backscattering induced noise is based on the Pound–Drever–Hall (PDH) technique[17]. The RFOG system is shown by Fig. 1: the PM1 and PM2 are the phase modulators, and PD1 and PD2 are the photodetectors (PDs).

After the phase of the incident beam is modulated by the phase modulators (PM1 and PM2), the electric field can be described as

$$E_{\mathrm{inc}} = E_0\, e^{i(\omega t + \beta \sin \Omega t)}. \tag{1}$$

 © 2018 Chinese Optics Letters

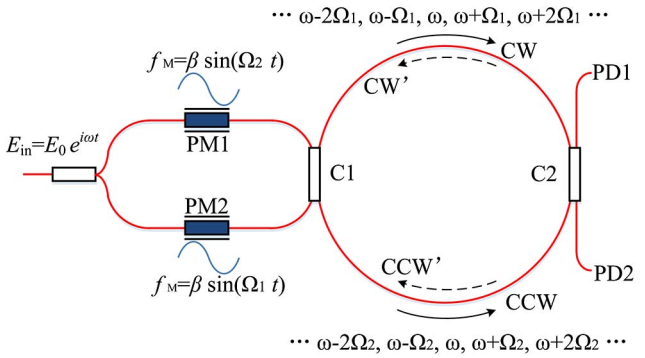


Fig. 1. Illustration of the RFOG system and the frequency components in the CW and CCW directions. C1 and C2: couplers.

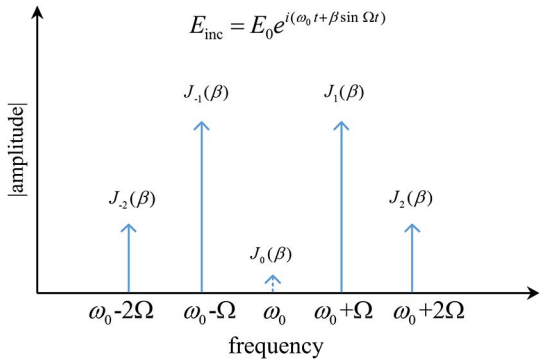


Fig. 2. Spectrum after the phase is modulated, and the carrier component $\omega_0$ is suppressed.

By using Bessel functions, the expression can be expanded to

$$E_{\text{inc}} \approx E_0[J_0(\beta) + 2iJ_1(\beta)\sin \Omega t]e^{i\omega t} = E_0[J_0(\beta)e^{i\omega t} + J_1(\beta)e^{i(\omega+\Omega)t} - J_1(\beta)e^{i(\omega-\Omega)t}], \quad (2)$$

where $\Omega$ is the phase modulation frequency and $\beta$ is the modulation depth. The signal detected by PD1 and PD2 can be described as:

$$\begin{aligned} P_{\text{ref}} = {} & P_c|F(\omega)|^2 + P_s[|F(\omega+\Omega)|^2 + |F(\omega-\Omega)|^2] \\ & + 2\sqrt{P_c P_s}\{\text{Re}[F(\omega)F^*(\omega+\Omega) \\ & - F^*(\omega)F(\omega-\Omega)]\cos \Omega t \\ & + \text{Im}[F(\omega)F^*(\omega+\Omega) - F^*(\omega)F(\omega-\Omega)]\sin \Omega t\} \\ & + (2\Omega\text{terms}), \end{aligned} \quad (3)$$

where $F(\omega)$ is the transmission coefficient of the RFOG, and $P_c$ and $P_s$ are the power in the carrier and the first-order sideband, respectively.

The form of Eq. (2) shows that there are actually different beam components incident on the cavity: a carrier, with angular frequency $\omega$, and the sidebands with angular frequencies $\omega \pm \Omega$, $\omega \pm 2\Omega$, $\omega \pm 3\Omega$..., as shown in Fig. 1. According to Eqs. (1) and (2), after the phase modulator, the single frequency beam is split into a series of equal-interval frequency components. The amplitude of each component is a function of $\beta$. The output spectrum after the phase modulator is shown in Fig. 2.

Therefore, we can equivalently take the phase-modulated beam as a series of beams with different frequencies incident on the ring cavity of the RFOG. As shown in Fig. 1. The CW′ and CCW′ are the backscattering or backreflection beams of CW and CCW beams, respectively. However, for example, the CW′ beams will interfere with the CCW beams, which will cause errors in the demodulation of PD1. To avoid the interference between the CW′ and CCW beams, different modulation frequencies $\Omega_1$ and $\Omega_2$ are applied on PM1 and PM2. Then the spectra of CW′ and CCW will have an offset to each other except $\omega_0$ frequency, and the interference between the sidebands will be eliminated by a circuit filter.

But the center frequency $\omega_0$ of the laser, which is called the carrier frequency, is still a common frequency in both the CW and CCW directions. To solve the problem of the carrier interference between CW′ and CCW, the carrier must be suppressed by choosing a proper modulation depth $\beta$, which makes the carrier amplitude $J_0(\beta) = 0$. Figure 2 also shows the spectrum when the carrier component is suppressed.

As mentioned above, to eliminate the interference with backscattering, different modulation frequencies $\Omega$ and specific modulation depths $\beta$ are adopted. However, the amplitude of the carrier may not be suppressed to 0 for the extremely high requirement for modulating accuracy and some errors, such as device parameters and voltage loss on wire, will also deteriorate the suppression performance. Additional modulation frequencies can be used to further suppress the carrier. Here we propose a new scheme to further realize the carrier suppression and the elimination of the interference between sidebands (CW′ and CCW, CW and CCW′). The scheme is shown in Fig. 3.

The resonant cavity can be taken as a bandpass filter. From Fig. 1 and the discussions above, we know that the carrier is the unique common frequency component in the CW and CCW directions when using different modulation

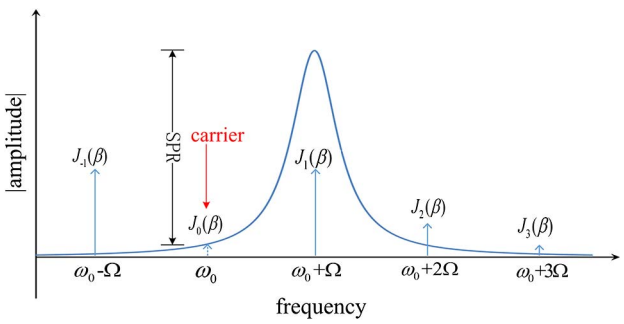


Fig. 3. Illustration of carrier suppression by locking the sideband to the cavity resonance.

frequencies. Thus, we can lock the sideband $(\omega_0 + \Omega)$ to the cavity resonance, as shown in Fig. 3. With proper modulation frequency $\Omega$, the carrier component (labeled by the arrow and carrier) will locate at the stop band, and the SPR indicates the suppression scale. The whole scheme is shown in Fig. 4.

Figure 4 shows both the CW and CCW spectra. In conclusion, the characteristics of the scheme can be described as follows. At first, the CW and CCW carrier components are sufficiently suppressed by choosing $\beta$ accurately to make $J_0(\beta) \to 0$. Then the sideband is locked to the resonance to make the carrier stay at the stop band of the cavity, thus the carrier is further suppressed. As a result, the interference between the carrier and its backscattering from the opposite direction can be greatly reduced. Second, with different modulation frequencies, the sideband CW and CCW spectra have an offset to each other, as shown in Fig. 4. The result is that the difference in CW and CCW frequency generates the beating, which will be filtered out sufficiently in the signal processing. Thus, influence of backscattering induced noise is eliminated.

Here, for example, we can set $\Omega = 2\pi \cdot 5 \cdot \mathrm{FWHM}$ (FWHM: full width at half-maximum). According to the simulation of a resonant fiber optical gyro with a finesse of 50, the amplitude of the carrier frequency can be suppressed additionally by 25 dB by the resonant cavity itself. The scheme is compatible with currently used devices in the RFOG system and requires less control accuracy to suppress the carrier. With the increase of the demodulation frequency or the decrease of FWHM, the SPR will increase.

Another important issue is the design of modulation frequencies $\Omega_1$ $(f_{M1})$ and $\Omega_2$ $(f_{M2})$ in the CW and CCW directions. According to experiment, the demodulation curve has many linear parts near each sideband frequency component when the demodulation signal has a proper phase offset to the PD signal. The linear parts are just the regions where the RFOG works. Both CW and CCW demodulation curves are shown in Fig. 5.

As shown in Fig. 5, for the use of different modulating frequencies, the linear parts have an offset to each other between the CW and CCW directions. If the offset is large, the system may not work as a linear rotation sensor when

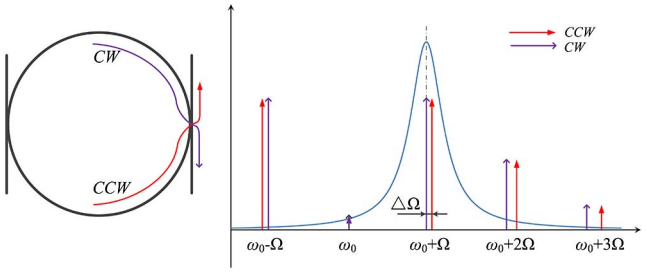


Fig. 4. (Color online) Whole scheme when sideband locking and different modulation frequencies are applied to the system.

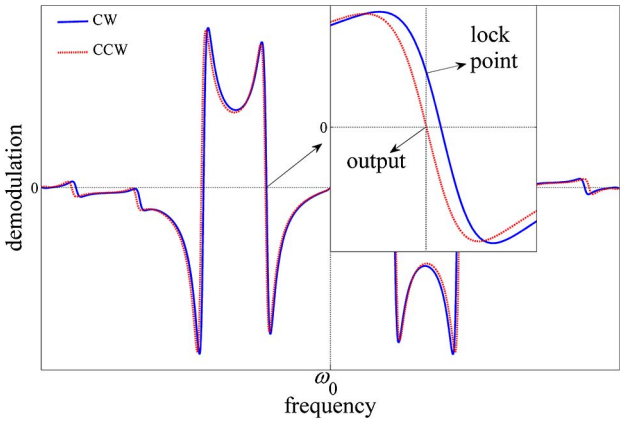


Fig. 5. (Color online) CW/CCW demodulation and the locking scheme when different modulation frequencies are adopted.

one direction is locked to a monotonic interval, so the choice of $\Omega_1$ and $\Omega_2$ must meet two conditions.

First, the linear parts of the CW and CCW demodulation curves must have enough overlapping range. Therefore, when the gyro output is linear, it can also ensure a monotonic interval for proportional–integral–derivative (PID) locking of the opposite direction. In Fig. 5, the child window shows the magnified linear and overlapped region. In the CW direction, we can set a lock point that has an offset to zero while the gyro output in the CCW direction is exactly linear, as shown by the arrows in the child widow. The final gyro output can be the difference between the output and the lock point to suppress the locking noise.

Second, the difference $|\Omega_1 - \Omega_2|$ must be large enough so that the beat frequency can be filtered out by a lowpass filter after the mixer. According to the simulation and experiments, the difference in CW and CCW modulating frequencies can be great enough that the beat frequency can be filtered out and it also meets the requirement of the first condition at the same time.

The modulation and demodulation system is shown in Fig. 6. Figure 6 only shows the CW demodulation process; a phase shifter must be used for adjusting the phase

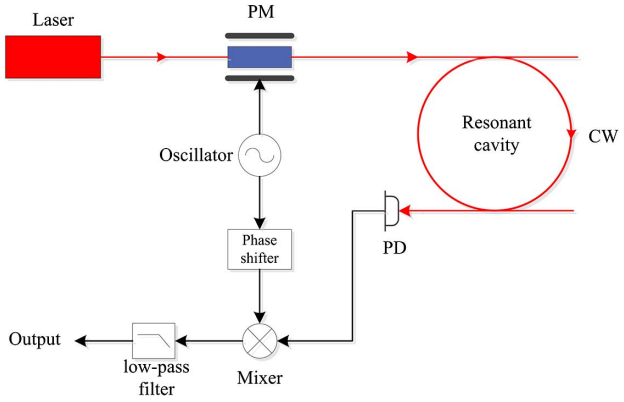


Fig. 6. CW modulation and demodulation system.

difference between the PD signal and the oscillator signal, since the demodulation curve varies with the phase difference. In fact, the functions such as the oscillator, phase shifter, mixer and filter, can be realized by a field-programmable gate array.

The wavelength of the laser $\lambda = 1550$ nm, the cavity length $L = 6$ m, FSR $= 33.3$ MHz, FWHM $= 610$ kHz, $V_\pi = 5.75$ V. Figure 7 shows the measurement result of the SPR of an RFOG; the $x$ axis indicates the deviation between the laser frequency and the resonant frequency of the cavity. We can see that the SPR can reach 19.87 dB when the carrier frequency locates at the position five times that of the FWHM away from the resonant frequency of the cavity. With the deviation increase, the SPR can reach 25 dB. In theory, the ideal modulation depth that makes the carrier amplitude $J_0(\beta') = 0$, is $\beta' \approx 2.405$, and the corresponding voltage parameter of the modulation frequency is $V_{\text{pp}} = 8.8$ V. According to the experiment, the amplitude varies within the range from $-5$ to $+5$ mV, so the error percent is 5 mV/(8.8 V/2) $\approx 1\%$. The corresponding SPR of the carrier amplitude is $20 \cdot \log\left(\frac{J_0(0)}{J_0[\beta'(1\pm1\%)]}\right) \approx 38$ dB, thus the total SPR $> 19.87 + 38 = 57.87$ dB when $\Omega > 2\pi \cdot 5 \cdot$ FWHM, and the corresponding intensity SPR is 115.74 dB.

With the proper phase difference in the experiment, we can obtain the curves shown in Fig. 8.

In Fig. 8, curve (1) is the driving voltage applied to the laser to change the frequency. Curve (2) is the output power of the sidebands detected by PD. Curve (3) is the demodulation of the cosine term while curve (4) is the demodulation of the sine term in Eq. (3). Curve (3) is just the curve we need to implement the sideband locking scheme, and curve (4) can be taken as the auxiliary flag for locking the sideband to the resonance. There is a linear part in curve (3) near every sideband. The sidebands can be considered to be locked to the resonance when the value of curve (4) is greater than 75% of the height, and positive or negative feedback

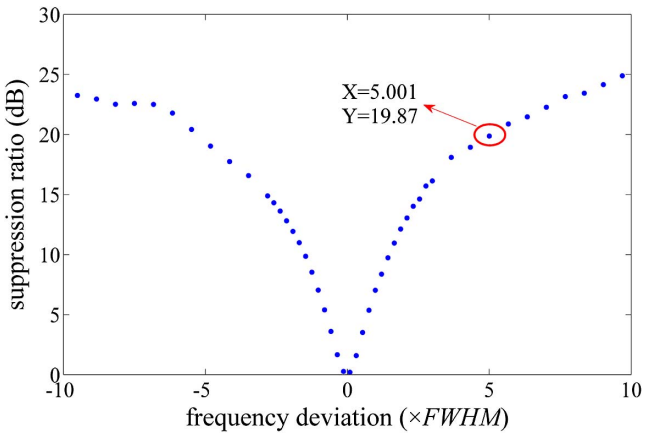


Fig. 7. SPR measurement of the cavity.

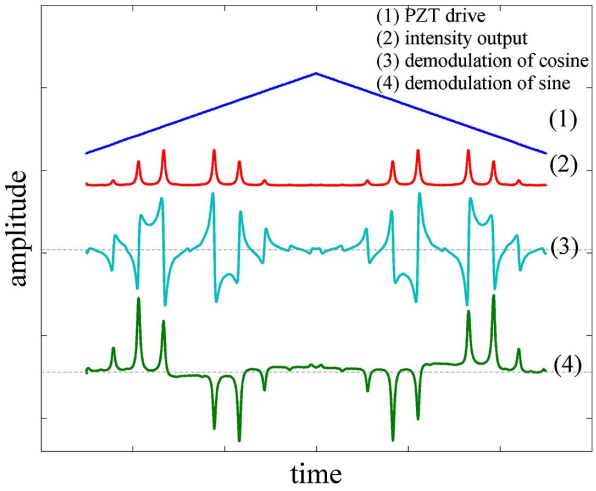


Fig. 8. (Color online) Curves obtained in the experiments. (1) The PZT driving voltage on the laser; (2) the intensity output detected by PD; (3) the demodulation of the cosine term of Eq. (3); (4) the demodulation of sine term of Eq. (3).

of PID distinguishes which sideband of the 1st and 2nd sidebands is locked to the resonance. In practice, to get curve (3), the phase difference between the input signals of the mixer should be adjusted in advance. The modulation CW and CCW frequencies are set at 3.5 and 3.56 MHz, respectively, and the corresponding demodulation curves obtained in the experiment are shown in Fig. 9.

The demodulation is shown on the left side of Fig. 9, and the linear part surrounded by an ellipse is magnified and shown in the right. The difference in the modulation frequencies is 60 kHz, which is out of the bandwidth of the lowpass filter (bandwidth = 1 kHz), so the interference between the sideband and sideband backscattering can be considered to be filtered out absolutely. The overlapped and linear range can also help to reduce the locking noise by subtracting between CW and CCW. The experiment results are shown in Fig. 10.

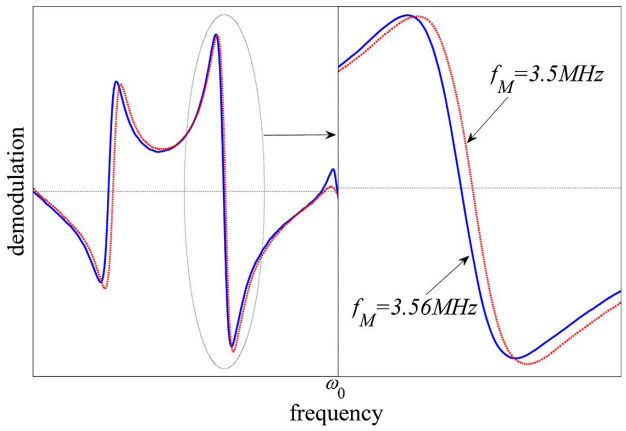


Fig. 9. (Color online) Demodulation curves obtained from experiments. The CW and CCW modulation frequencies are 3.5 MHz and 3.56 MHz, respectively. The right window is the magnification of the part in the ellipse.

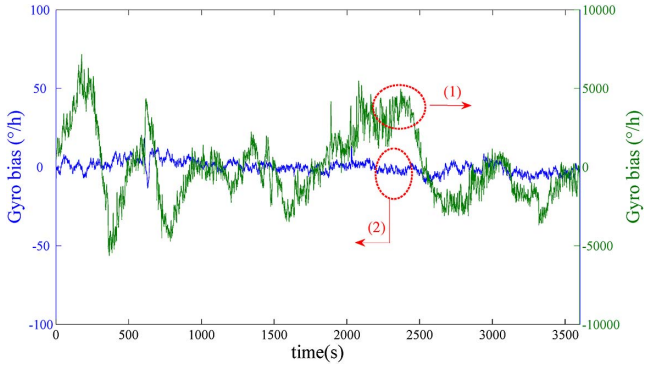


Fig. 10. (Color online) Comparison of experiment results. The value of curve (1) is shown by the right axis while curve (2) is shown by the left axis.

Curve (1) shows the result when non-sideband locking is adopted, that is locking the carrier to the resonance, and the carrier is not suppressed ($\beta = 1.08$[17], when max sensitivity can be obtained). Curve (2) shows the result when the sideband locking technique is adopted. Curve (1) varies in a larger scale compared with curve (2), and the result is improved greatly when the carrier and backscattering induced noise are suppressed. By sideband locking, the bias stability is improved from 0.47°/s to 0.0042°/s over one hour with an integration time of 10 s. Therefore, carrier and backscattering play an important part in deteriorating the performance.

In conclusion, by the sideband locking scheme, the total intensity SPR of the carrier component can reach 115.74 dB and the backscattering induced noise of the sidebands is eliminated for the adoption of different modulation frequencies. However, the RFOG still suffers from polarization fluctuation induced noise, which is one dominant error in the gyro, and the stability of the high modulation frequency will also directly affect the performance. The result will be further improved when the former factors can be improved. The high modulation frequency is more sensitive to the phase fluctuation, for which we will propose a detailed solution in subsequent work. The scheme provides a new idea for the suppression of backscattering induced noise.

## References

1. G. Sagnac, C. R. Acad. Sci. **157**, 708 (1913).
2. H. J. Arditty and H. C. Lefevre, Opt. Lett. **6**, 401 (1981).
3. X. Jiang, X. Li, H. Zhang, and A. Y. Wang, Chin. Opt. Lett. **14**, 070201 (2016).
4. Y. Yang and F. Yang, Chin. Opt. Lett. **14**, 110605 (2016).
5. K. Suzuki, K. Takiguchi, and K. Hotate, in *Photonics East (ISAM, VVDC, IEMB)* (1999), p. 66.
6. G. A. Sanders, M. G. Prentiss, and S. Ezekiel, Opt. Lett. **6**, 569 (1981).
7. R. E. Meyer, S. Ezekiel, D. W. Stowe, and V. J. Tekippe, Opt. Lett. **8**, 644 (1983).
8. K. Iwatsuki, K. Hotate, and M. Higashiguchi, Appl. Opt. **23**, 3916 (1984).
9. K. Hotate, K. Takiguchi, and A. Hirose, IEEE Photonics Technol. Lett. **2**, 75 (1990).
10. K. Suzuki, K. Takiguchi, and K. Hotate, J. Lightwave Technol. **18**, 66 (2000).
11. K. Suzuki, K. Takiguchi, and K. Hotate, Electron. Lett. **35**, 1076 (1999).
12. K. Suzuki, K. Takiguchi, and K. Hotate, in *Optical Fiber Sensors* (1999), p. 78.
13. H. Ma, Z. He, and K. Hotate, J. Lightwave Technol. **29**, 85 (2011).
14. H. Mao, H. Ma, and Z. Jin, Opt. Express **19**, 4632 (2011).
15. L. Feng, M. Lei, H. Liu, Y. Zhi, and J. Wang, Appl. Opt. **52**, 1668 (2013).
16. J. Wang, L. Feng, Y. Zhi, H. Liu, W. Wang, and M. Lei, Appl. Opt. **52**, 7712 (2013).
17. E. D. Black, Am. J. Phys. **69**, 79 (2001).